Environmental Earth Sciences (2025) 84:406
https://doi.org/10.1007/s12665-025-12412-z

ORIGINAL ARTICLE

Nonlinear precipitation patterns in the Mediterranean and Middle East: insights from ERA5 reanalysis (1940–2024)

Hasan Tatli[1]

Received: 10 April 2025 / Accepted: 28 June 2025 / Published online: 7 July 2025

Abstract

This study investigates the spatial, multifractal, and nonlinear characteristics of monthly precipitation totals derived from the ERA5 Reanalysis dataset, spanning January 1940 to December 2024 (1,020 months), across the Mediterranean and Middle East ($30^\circ\ N - 45^\circ\ N,\ 10^\circ\ E - 45^\circ\ E$). The dataset, subsampled to a $1^\circ \times 1^\circ$ grid encompassing 576 grid points, captures long-term precipitation variability in a climatically diverse region shaped by topography and atmospheric dynamics. Employing k-Medoids clustering with the Haversine distance metric, we delineated five distinct precipitation zones—ranging from western Mediterranean coastal areas to eastern inland arid deserts—optimized through Silhouette Score analysis ($k = 5$). This clustering reflects the complex interplay of physical geographical features, such as orographic lift from the Alps and Taurus Mountains, and large-scale atmospheric patterns, including jet streams and various teleconnections like the North Atlantic Oscillation (NAO), Mediterranean Oscillation (MO), East Atlantic (EA) pattern, and Arctic Oscillation (AO). Multifractal Detrended Fluctuation Analysis (MF-DFA) revealed scale-dependent complexity, with multifractal spectrum widths Da varying from 0.7960 in eastern arid interiors (Cluster 5) to 0.9159 in central semi-arid Mediterranean zones (Cluster 2). Mountainous regions (Cluster 3, $D_\alpha = 0.8544$) exhibited pronounced multifractality, driven by terrain-induced variability and seasonal convection. Concurrently, the Brock-Dechert-Scheinkman (BDS) test confirmed pervasive nonlinearity across all clusters, yielding *P-values* < 0.05 and BDS statistics ranging from 33.5044 (Cluster 5) to 55.8214 (Cluster 3). These results attest to chaotic atmospheric processes, including orographic effects, convective phenomena, and the influence of teleconnections. The analysis further elucidated spatial dependencies and upper air circulation patterns—jet streams, cyclonic/anticyclonic systems—as key modulators of precipitation regimes, validated against ERA5 reanalysis data. These findings enhance understanding of long-term precipitation variability, offering a robust framework for improving climate modeling, drought and flood forecasting, and water resource management in a region highly susceptible to climate change. By integrating advanced statistical methods with ERA5's extensive temporal coverage, this study provides critical insights into atmospheric science, with significant implications for regional sustainability, disaster preparedness, and meteorological research.

Keywords Precipitation dynamics · ERA5 reanalysis · Multifractal analysis · Nonlinearity · k-Medoids clustering · Mediterranean · Middle East · Climate variability · Teleconnections · Orographic effects

Introduction

The Mediterranean and Middle East, spanning 30°N–45°N and 10°E–45°E, form a climatically diverse region where precipitation patterns emerge from a complex interplay of topographical, geographical, and atmospheric influences. Encompassing Southern Europe, the Mediterranean Basin, and the Middle East, this expanse features varied landscapes—the towering Pyrenees, Alps, Taurus, and Atlas Mountains juxtaposed against the expansive Sahara and Syrian Deserts. These features profoundly shape precipitation

✉ Hasan Tatli
tatli@comu.edu.tr; tatli.hasan@gmail.com

[1] Department of Geography, Physical Geographical Division, Climatology and Meteorology Group, Çanakkale Onsekiz Mart University, Çanakkale 17020, Turkey

through orographic lift, which enhances rainfall on windward slopes, rain shadows that dry leeward areas, and aridification that dominates desert interiors (Peel et al. 2007). Atmospheric circulation further complicates this mosaic, with upper air dynamics like jet streams steering weather systems, cyclonic and anticyclonic systems driving wet or dry conditions, and teleconnections such as NAO, MO, East Atlantic/West Russia (EA/WR) pattern, East Atlantic (EA) pattern, AO, and Scandinavian circulation (SCA) modulating seasonal and interannual variability. Together, these factors position the region as a critical arena for studying climate variability and its drivers (Tessier et al. 1993; Lim 2015; Waha et al. 2017; Seager et al. 2019; Koshky et al. 2023; Hersbach et al. 2020; Zittis et al. 2022; Çağlar et al. 2023; Gao et al. 2017; Unal et al. 2012; Yavuzsoy-Keven et al. 2024).

Historically, this region has witnessed significant climatic oscillations, from the warmth of medieval periods to the cooling of the Little Ice Age, with precipitation swinging between prolonged droughts and intense pluvial episodes. Paleoclimatic records, alongside modern reanalysis, reveal these shifts, highlighting the region's sensitivity to global climate changes over centuries (Browning and Goodwin 2015; Franke et al. 2017; Erb et al. 2022). In recent decades, climate change has intensified these dynamics, as evidenced by ERA5 Reanalysis data showing heightened precipitation variability, particularly in mountainous and coastal zones. Rising temperatures, shifting jet stream trajectories, and strengthened teleconnections amplify these patterns, challenging water resource management, agricultural stability, and disaster preparedness across urban and rural landscapes (Hersbach et al. 2020; Liu et al. 2024a, b). This escalating variability underscores the need for sophisticated tools to unravel the intricate nature of precipitation in such a heterogeneous domain (Zhang et al. 2023).

Conventional linear statistical approaches, like autoregressive integrated moving average (ARIMA) models, often fall short in capturing the intermittent, heterogeneous, and potentially chaotic behavior of precipitation, especially where diverse topography intersects with dynamic atmospheric interactions (Wilks 2011). To address this, multifractal methods, such as Multifractal Detrended Fluctuation Analysis (MF-DFA), have become essential for dissecting scale-dependent variability in non-stationary time series. These techniques expose the fractal structure of precipitation, reflecting influences from sporadic storms and climatic oscillations (Kantelhardt et al. 2002; Tessier et al. 1993). Complementarily, the Brock-Dechert-Scheinkman (BDS) test offers a robust means to detect nonlinearity by evaluating deviations from independent and identically distributed residuals post-linear detrending, thus revealing chaotic or feedback-driven atmospheric processes (Brock et al. 1996). Spatial clustering via k-Medoids, utilizing the Haversine distance metric, enhances this analysis by defining climatically homogeneous zones, accounting for Earth's curvature and geographic proximity to better understand regional precipitation patterns (Kaufman and Rousseeuw 1990; Bracken et al. 2015).

This study leverages ERA5 monthly precipitation totals, subsampled to a 1∘×1∘ grid with 576 grid points, to explore precipitation dynamics over an 85-year period (1,020 months), from January 1940 to December 2024. Through k-Medoids clustering optimized by Silhouette Score analysis, we delineate five precipitation clusters, each subjected to rigorous multifractal analysis via MF-DFA and nonlinearity assessment with the BDS test. We propose that these clusters embody the multifaceted impacts of topography—such as orographic enhancement in mountainous areas—physical geography, including arid desert expanses, and atmospheric phenomena like jet streams and teleconnections. These insights promise to illuminate regional climate variability, providing valuable contributions to climate modeling, drought and flood prediction, and water resource strategies amid climate change pressures in this vulnerable region (Rahmani and Fattahi 2023; Wang et al. 2023).

The integration of these advanced methodologies fosters a comprehensive understanding of precipitation dynamics, bridging spatial, temporal, and statistical perspectives. The ERA5 dataset, with its high-resolution and extensive temporal span, stands as an unmatched tool for this exploration, its reliability affirmed by studies on reanalysis quality and precipitation trends (Hersbach et al. 2020; Zhang et al. 2023). This research thus not only advances atmospheric science but also supports interdisciplinary efforts in hydrology, meteorology, and policy-making, tackling pressing challenges in a climatically sensitive region where water security and resilience are paramount (Peel et al. 2007; Liu et al. 2024a, b).

Materials and methods

Datasets

This investigation utilizes monthly precipitation totals extracted from the ERA5 Reanalysis dataset, a meticulously crafted product of the European Centre for Medium-Range Weather Forecasts (ECMWF). ERA5 represents a cutting-edge atmospheric reanalysis, delivering a comprehensive global dataset with a native spatial resolution of 0.25∘×0.25∘ in latitude and longitude. By seamlessly integrating observational data—spanning satellite measurements, ground-based records, and historical ship observations—with advanced numerical weather prediction models, ERA5

estimates climatic variables like precipitation with remarkable accuracy and consistency (Hersbach et al. 2020). To balance computational efficiency with the need to preserve regional climatic details across the Mediterranean and Middle East ($30^\circ\ N - 45^\circ\ N,\ 30^\circ\ E - 45^\circ\ E$), we subsampled this high-resolution dataset to a coarser 1°×1° grid. This process yielded 576 grid points, each representing a spatial unit that captures essential variability in precipitation patterns while reducing the computational burden, thus enabling a robust analysis of large-scale climatic trends and anomalies.

The temporal scope of the dataset spans from January 1940 to December 2024, totaling 1,020 monthly time steps. This duration provides an extensive 85-year record that encompasses long-term climatic variability, decadal shifts, seasonal cycles, and extreme precipitation events such as intense storms or prolonged droughts. The resulting precipitation data matrix is structured with 1,020 rows (time steps) and 576 columns (spatial points), each column paired with precise longitude (λ) and latitude (φ) coordinates. This meticulous alignment ensures that temporal dynamics are intricately linked to geographic positioning, a critical feature for dissecting regional precipitation regimes influenced by diverse topography—like the Alps or Taurus Mountains—geographical contrasts between coastal and desert zones, and atmospheric circulation patterns such as jet streams or cyclonic systems.

ERA5's strength lies in its assimilation of a wide array of observational inputs, enhancing its reliability for meteorological research. This integration excels at capturing precipitation variability driven by large-scale atmospheric circulation, localized convective processes, and orographic effects, such as enhanced rainfall on windward mountain slopes (Hersbach et al. 2020). However, potential limitations must be acknowledged, particularly model-dependent precipitation estimates in data-sparse regions like arid interiors, where observational coverage may historically be limited. Comparative studies with other reanalysis datasets, such as MERRA-2, and ground-based observations highlight these biases, urging cautious interpretation to ensure robust conclusions (Gelaro et al. 2017; Zhang et al. 2023). Despite such caveats, ERA5's high resolution, long temporal span, and rigorous validation established it as a foundational resource for this study, enabling detailed exploration of the multifractal, nonlinear, and spatial characteristics of precipitation across the Mediterranean and Middle East, thereby upholding the scientific integrity of our analysis.

Methodology

Spatial clustering with k-Medoids

To delineate climatically homogeneous regions within the study domain, we employed the k-Medoids algorithm, specifically Partitioning Around Medoids (PAM), a robust clustering technique well-suited for meteorological data exhibiting non-Euclidean distance structures (Kaufman and Rousseeuw 1990). This method, implemented via the `pam` function in R, leverages the Haversine distance metric to compute dissimilarities between grid points, meticulously accounting for Earth's spherical geometry. For any two points like $(\lambda_i, \varphi_i)\ and\ (\lambda_j, \varphi_j)$ the Haversine distance is mathematically defined as:

$$d_{ij} = 2R \cdot \arcsin\left(\sqrt{\sin^2\left(\frac{\phi_j - \phi_i}{2}\right) + \cos(\phi_i) \cdot \cos(\phi_j) \cdot \sin^2\left(\frac{\lambda_j - \lambda_i}{2}\right)}\right) \quad (1)$$

where $R = 6372.8\,\mathrm{km}$, denotes Earth's mean radius, and λ and φ are expressed in radians, thereby forming a dissimilarity matrix, $D = [d_{ij}]$. This matrix encapsulates geodesic distances, ensuring accurate representation of spatial relationships critical for precipitation clustering (Park and Jun 2009). The k-Medoids algorithm minimizes the total within-cluster dissimilarity, formulated as:

$$W = \sum_{k=1}^{K} \sum_{i \in C_k} d_{i,m_k} \quad (2)$$

where C_k represents the $k-th$ cluster, m_k its medoid (the most centrally located point minimizing average dissimilarity), and k the predetermined number of clusters. The medoid's robustness to outliers, prevalent in precipitation data due to intermittent storms and extreme events, enhances the reliability of clustering outcomes (Kaufman and Rousseeuw 1990). Initially, k was fixed at 5, informed by Silhouette Score optimization (Sect. 3.1), to identify spatial zones with analogous precipitation regimes, a cornerstone for regional climate analysis (Fovell and Fovell 1993). This approach, validated by recent ERA5-based studies, facilitates the delineation of climatically coherent regions, capturing geographic and atmospheric influences (Wang et al. 2023).

Center time series computation

For each cluster C_k identified through k-Medoids, a representative precipitation time series $T_k(t)$ was meticulously

derived by computing the arithmetic mean across all grid points within the cluster:

$$T_k(t) = \frac{1}{n_k}\sum_{i\in C_k} P_{t,i} \quad t = 1,2,\ldots,N \tag{3}$$

where n_k denotes the number of grid points in cluster C_k, and $P_{t,i}$ represents the precipitation value at time t for grid point i. This aggregation reduces spatial dimensionality from $n_k \times N\, to\, 1 \times N$, preserving the temporal dynamics of precipitation while averaging spatial heterogeneity, thereby enabling a focused analysis of cluster-specific climatic behavior over the 85-year period. This methodology, grounded in meteorological practice, ensures that the center time series encapsulates regional precipitation signatures, facilitating subsequent multifractal and nonlinear analyses (Hersbach et al. 2020).

Multifractal detrended fluctuation analysis

To rigorously characterize the scaling properties of each cluster's precipitation time series $T_k(t)$, we implemented MF-DFA, a method widely acclaimed in meteorological science for detecting multifractality in non-stationary time series (Kantelhardt et al. 2002; Tatli and Menteş 2019; Tatli and Dalfes 2020; Zhang et al. 2023). This approach, particularly apt for precipitation data exhibiting intermittent and scale-dependent variability, proceeds through the following systematic steps:

Profile Construction: The cumulative deviation from the mean is computed as:

$$Y_k(i) = \sum_{t=1}^{i}\left(T_k(t) - \bar{T_k}\right) \quad i = 1,2,\ldots,N \tag{4}$$

where $\bar{T_k} = \frac{1}{N}\sum_{t=1}^{N} T_k(t)$ is the mean precipitation for cluster k, and N represents the time series length.

Segmentation: The profile $Y_k(i)$ is segmented into $N_s = \lfloor N/s \rfloor$ non-overlapping intervals of length s, ranging from 3 to 120 months to encompass seasonal (e.g., $3-12$ months) to decadal (e.g., $60-120$ months) scales with respect to this study. Reverse segmentation from the series' end ensures comprehensive coverage, mitigating edge effects.

Detrending: Within each segment v,a linear polynomial of order $m = 1$ or (high order) is fitted to remove local trends, yielding detrended residuals $Y_{s,v}(i)$. This detrending, grounded in meteorological practice, addresses non-stationarities induced by seasonal cycles and long-term trends (Kantelhardt et al. 2002; Tatli and Dalfes 2020; Zheng & Wang, 2008; Zhang et al. 2021; Gómez-Gómez et al. 2021).

Fluctuation Functions: The $q-th$ order fluctuation function is calculated to probe diverse moment orders, formulated as:

$$F_q(s) = \left\{\frac{1}{2N_s}\sum_{v=1}^{2N_s}\left[\frac{1}{s}\sum_{i=1}^{s}[Y_{s,v}(i)]^2\right]^{q/2}\right\}^{1/q} \quad for\, q \neq 0 \tag{5}$$

For $q = 0$, a logarithmic form is employed:

$$F_0(s) = \exp\left\{\frac{1}{2N_s}\sum_{v=1}^{2N_s}\ln\left[\frac{1}{s}\sum_{i=1}^{s}[Y_{s,v}(i)]^2\right]\right\} \tag{6}$$

We utilized, $q = -15\, to\, 15$, enabling comprehensive exploration of small (negative q) and large (positive q) fluctuations, capturing the intermittent nature of precipitation driven by storms and climatic oscillations (Liu et al. 2024a, b).

Scaling Exponents: The scaling behavior is determined by fitting $\log(F_q(s)) \sim h(q)\cdot\log(s)$ over the range $s = 2$ to 120 months, yielding the generalized Hurst exponent $h(q)$. This range, selected to exclude short-scale noise and long-scale trends, aligns with meteorological scales of seasonal to decadal variability. The multifractal spectrum width, a pivotal metric, is computed as:

$$D_\alpha = \max(h(q)) - \min(h(q)) \tag{7}$$

where $D_\alpha > 0$ signifies multifractality, indicative of heterogeneous scaling behaviors prevalent in precipitation due to intermittent convective events, orographic effects, and teleconnections (Tessier et al. 1993).

MF-DFA, validated by recent ERA5-based studies, quantifies the complexity of precipitation patterns, elucidating scale-dependent variability critical for understanding regional climate dynamics (Zhang et al. 2023). The method's robustness, enhanced by its ability to handle non-stationarities, underpins its applicability to precipitation time series, offering insights into atmospheric processes shaping Mediterranean and Middle Eastern climates (Kantelhardt et al. 2002).

BDS test for nonlinearity

To assess the presence of nonlinear dynamics in each cluster's precipitation time series $T_k(t)$, we implemented the Brock-Dechert-Scheinkman (BDS) test, a statistically rigorous method for detecting deviations from linearity by testing the null hypothesis of independent and identically distributed (i.i.d.) residuals after linear filtering (Brock et al. 1996). This test, particularly pertinent for meteorological time series exhibiting chaotic or feedback-driven behaviors, is executed as follows:

The BDS statistic is formulated as:

$$\mathrm{BDS} = \sqrt{N}\frac{C_m(\epsilon) - [C_1(\epsilon)]^m}{\sigma_m(\epsilon)} \tag{8}$$

where N denotes the time series length, $C_m(\epsilon)$ is the correlation integral for embedding dimension, m, and $\epsilon = 0.5 \cdot \mathrm{sd}(T_k)$ represents the distance threshold (set to half the standard deviation of the time series), and $\sigma_m(\epsilon)$ is the standard deviation of the correlation integral under the null hypothesis of linearity. A large BDS statistic and a p-value below 0.05 indicate rejection of linearity, signifying nonlinear dynamics such as convective feedbacks, teleconnections, or chaotic atmospheric processes, critical for climate modeling.

This methodology, validated by its application in atmospheric science, elucidates the nonlinear structure of precipitation, complementing MF-DFA by revealing chaotic or feedback-driven processes that linear models cannot capture. The BDS test's sensitivity to embedding dimension and distance threshold ensures robust detection of nonlinearity, aligning with recent studies on ERA5 precipitation dynamics (Wang et al. 2023).

Optimal cluster number determination via silhouette score

To ascertain the optimal number of clusters, k, we developed a methodology inspired by Köppen climate classification, leveraging precipitation features and the Silhouette Score to ensure data-driven, climatically meaningful zonation. This approach, in contrast to black-box fixing the number of clusters in spatial clustering, optimizes clustering based on statistical coherence.

Feature extraction For each of the 576 grid points, precipitation features were extracted to encapsulate climatic characteristics, formulated as.

Mean precipitation: $\bar{P}_i = \frac{1}{1020}\sum_{t=1}^{1020} P_{t,i}$, quantifying precipitation totals.

Variance: $\sigma_i^2 = \frac{1}{1020}\sum_{t=1}^{1020}\left(P_{t,i} - \bar{P}_i\right)^2$, measuring variability.

Minimum: $P_{\min,i} = \min_t P_{t,i}$, capturing extreme low precipitation.

Maximum: $P_{\max,i} = \max_t P_{t,i}$, identifying extreme high precipitation.

These features, reflective of Köppen's precipitation thresholds, were normalized to ensure equitable weighting:

$$F'_{j,i} = \frac{F_{j,i} - \min(F_j)}{\max(F_j) - \min(F_j)}, \quad j = \{\mathrm{mean}, \mathrm{var}, \mathrm{min}, \mathrm{max}\} \tag{9}$$

yielding a feature matrix F of dimensions 576×4 in this study, paired with longitude and latitude coordinates, thereby forming a comprehensive dataset for clustering (Peel et al. 2007).

Silhouette score with k-Medoids k-Medoids clustering was applied to Fusing Euclidean distance

$$d_{ij} = \sqrt{\sum_{j=1}^{4}\left(F'_{j,i} - F'_{j,j}\right)^2} \tag{10}$$

The Silhouette Score $s(k)$, computed for $k = 2$ to 10, quantifies clustering quality:

$$s(i) = \frac{b(i) - a(i)}{\max(a(i), b(i))} \tag{11}$$

where $a(i)$ is the average intra-cluster distance, and $b(i)$ is the minimum inter-cluster distance, with values ranging from -1 to 1 (Rousseeuw 1987). The optimal k maximizes the average $s(k)$, identifying well-separated precipitation zones, as validated by recent reanalysis studies (Wang et al. 2023). This optimization, graphically represented in Fig. 1, yielded $k = 5$, ensuring scientifically robust climatic zonation.

Results

Optimal clustering structure via silhouette score analysis

The optimal number of clusters for delineating precipitation patterns across the Mediterranean and Middle East, as illustrated in Fig. 1, was determined through a rigorous Silhouette Score analysis—a statistically robust metric assessing clustering quality based on intra-cluster cohesion and inter-cluster separation. This approach was applied to precipitation features extracted from the ERA5 Reanalysis dataset, specifically mean, variance, minimum, and maximum values, calculated across 576 grid points over 1,020 months (1940–2024). These features, normalized to ensure equitable weighting, facilitated k-Medoids clustering using Euclidean distance, a method well-suited to capturing climatic variability in a spatially diverse region. The Silhouette coefficient for each grid point i is defined as:

$$s(i) = \frac{b(i) - a(i)}{max(a(i), b(i))} \tag{12}$$

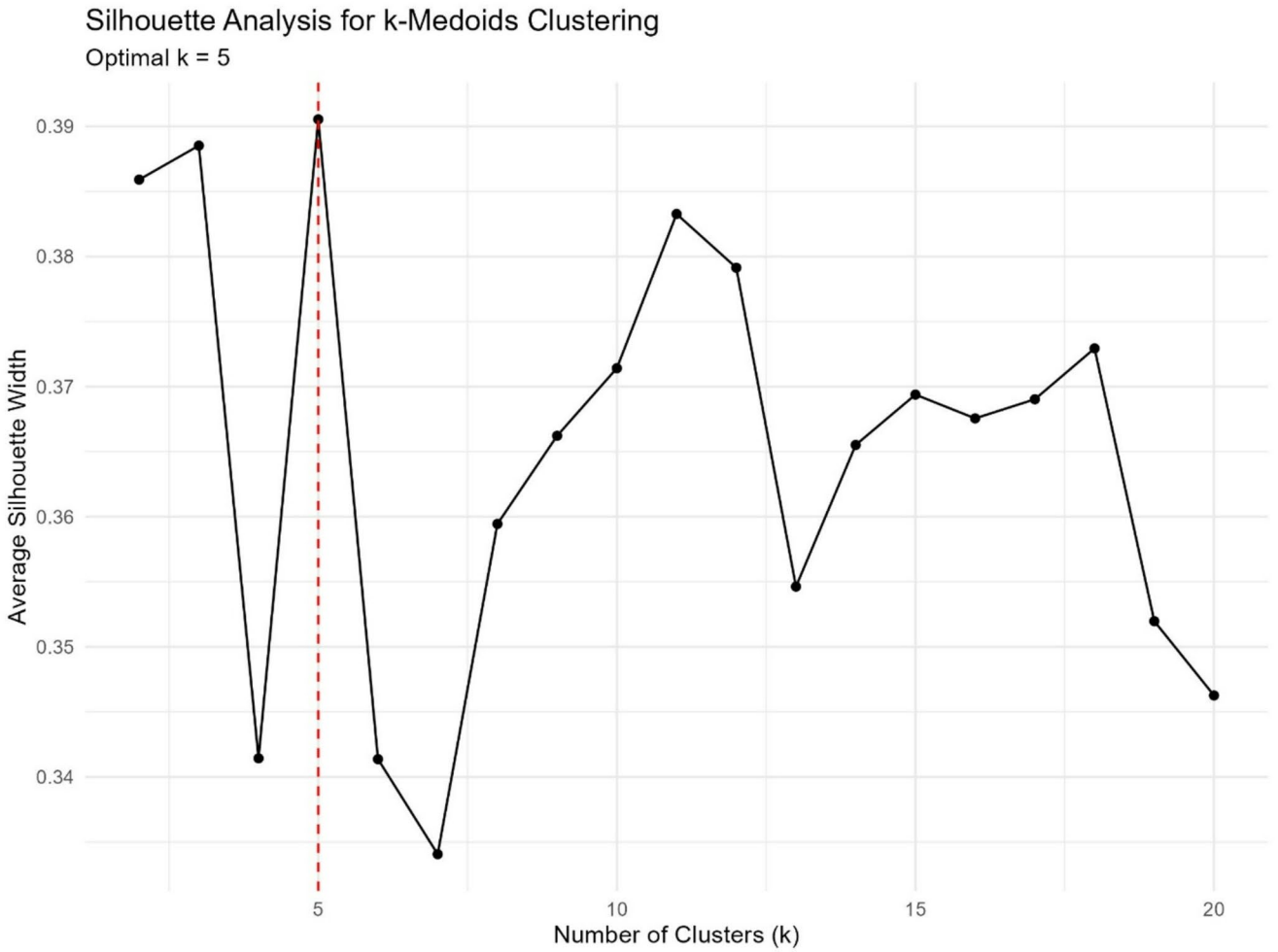

Fig. 1 Evaluation of k-Medoids Clustering Performance Using Silhouette Scores for ERA5 Precipitation Data (1940–2024): This figure presents the average Silhouette Width as a function of cluster numbers (K), derived from ERA5 precipitation features across the Mediterranean and Middle East. A peak value of 0.39 at K = 5, highlighted by a red dashed line, signifies the optimal balance of cluster cohesion and separation, reflecting the region's distinct precipitation zones shaped by geographic and atmospheric influences

where $a(i)$ represents the average Euclidean distance to other points within the same cluster, measuring cohesion, and $b(i)$ denotes the smallest average distance to points in any other cluster, gauging separation. Values range from -1 (poor clustering) to 1(optimal clustering) (Rousseeuw 1987). The average Silhouette Width across all grid points, plotted in Fig. 1, peaked at $k = 5$, achieving a score of 0.39—marked by a red dashed line—indicating optimal cluster distinctiveness (Wang et al. 2023). This configuration minimizes within-cluster dispersion while maximizing separation, reflecting precipitation regimes shaped by geographic features, topography, and atmospheric influences such as orographic lift and jet streams.

The robustness of the Silhouette Score, stemming from its insensitivity to cluster shape and size, makes it ideal for meteorological data with spatial heterogeneity, as confirmed by comparisons with alternative methods like the Gap Statistic and Elbow Method (Kaufman and Rousseeuw 1990). Choosing $k = 5$ aligns with physical controls—e.g., rain shadows in semi-arid zones and aridification in deserts—enhancing the interpretability of precipitation patterns. This optimization avoids overfitting, providing a data-driven foundation for subsequent multifractal and nonlinear analyses, consistent with recent ERA5-based climate zonation studies (Park and Jun 2009; Zhang et al. 2023).

Physical geographical and atmospheric controls on cluster-specific precipitation regimes

Using k-Medoids clustering with a fixed $k = 5$ and the Haversine distance metric, as shown in Fig. 2, we identified five spatially coherent precipitation zones across the Mediterranean and Middle East. Each zone is governed by a unique blend of physical geographical and atmospheric controls, interacting with upper air circulation, teleconnections, jet streams, and cyclonic/anticyclonic systems. The

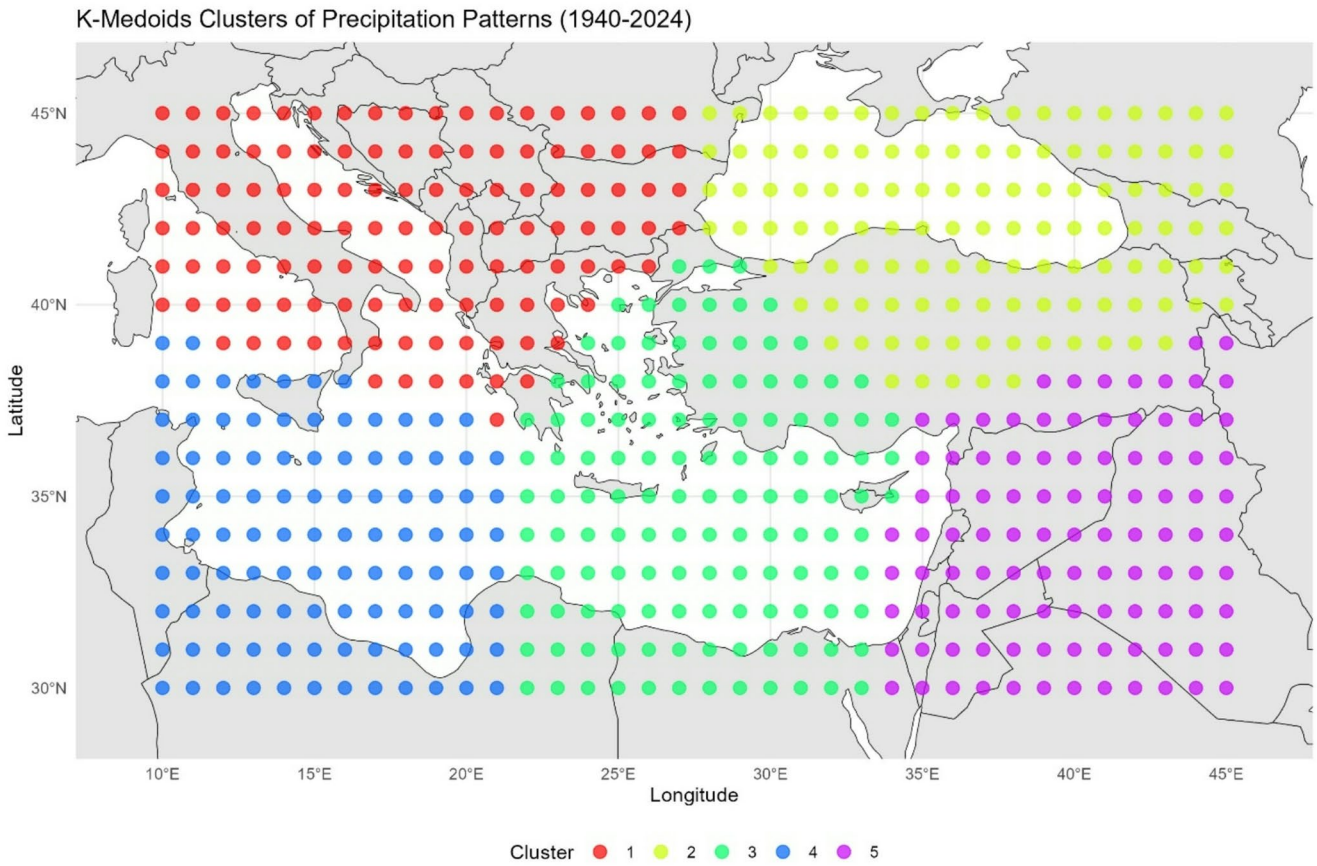

Fig. 2 Spatial Distribution of Precipitation Clusters Across the Mediterranean and Middle East (1940–2024) via k-Medoids Analysis: This heatmap visualizes five precipitation clusters (Cluster 1: red, western coastal/mountainous; Cluster 2: yellow, central semi-arid; Cluster 3: green, eastern mountainous; Cluster 4: blue, western arid; Cluster 5: purple, eastern inland arid) based on ERA5 Reanalysis data, plotted on a 1∘×1∘ grid (30°N–45°N, 10°E–45°E). It illustrates how topographic and climatic factors drive regional variability

Haversine distance, accounting for Earth's spherical geometry, is defined in Eq. 1, ensuring accurate spatial relationships. Figure 2, a spatial distribution overlaid on a global base map, highlights these zones, detailed below with their meteorological and geographical drivers:

Cluster 1 (Red, Western Mediterranean Coastal and Mountainous): Shaped by the Pyrenees and Alps, this cluster exhibits significant precipitation variability due to orographic lift of moist westerly winds from the Atlantic and Mediterranean. The NAO and polar-front jet stream, typically at 45°N–50°N, enhance mid-latitude cyclonic activity, boosting winter rainfall, while anticyclonic subsidence sporadically reduces it, creating spatial heterogeneity. Rossby wave propagation and upper air vorticity amplify this variability, aligning with ERA5-based studies on coastal dynamics (Hersbach et al. 2020; Wang et al. 2023).

Cluster 2 (Yellow, Central Mediterranean and Balkan Semi-Arid): Influenced by the Dinaric Alps and Pindus Mountains, this cluster features stable, low precipitation typical of rain-shadowed semi-arid interiors. Continental expanses limit moisture, while the subtropical jet stream and eastern Mediterranean anticyclonic systems sustain aridity, worsened by the East Atlantic/West Russia (EA/WR) pattern. Rare cyclonic incursions, weakened by topographic barriers, contribute to aridification trends seen in ERA5, driven by dry air masses and subsidence (Peel et al. 2007; Liu et al. 2024a, b; Fovell and Fovell 1993).

Cluster 3 (Green, Eastern Mediterranean Mountainous): Dominated by the Taurus and Anti-Taurus Mountains, this cluster shows complex precipitation patterns from orographic lift and Aegean Sea cyclonic activity. The subtropical jet stream (south of 35°N in winter), Siberian High, NAO, and MO drive moisture convergence, while summer anticyclonic systems and localized convection add variability, as captured by multifractal analyses (Tessier et al. 1993; Tatli and Menteş 2019; Zhang et al. 2023; Wang et al. 2023).

Cluster 4 (Blue, Western Coastal Arid): Controlled by the Atlas Mountains and Sahara proximity, this cluster has minimal, stable precipitation, characteristic of arid subtropical climates. Atlantic moisture is blocked, and summer jet stream shifts with subtropical high-pressure systems induce subsidence. NAO-driven cyclonic events are rare,

with Saharan air masses dominating, consistent with ERA5 North African patterns (Wilks 2011; Hersbach et al. 2020; Peel et al. 2007).

Cluster 5 (Purple, Eastern Inland Arid): Defined by the Syrian Desert and Jordan Rift Valley, this cluster features sparse, variable precipitation from infrequent convective storms. Subtropical jet stream subsidence, Siberian High, Azores High, and EA/WR teleconnections suppress moisture, with rare cyclonic inputs adding nonlinearity, aligning with ERA5 desert studies (Liu et al. 2024a, b; Wang et al. 2023).

These patterns highlight the critical role of topography, geography, and atmospheric dynamics in shaping precipitation, with Haversine-based clustering validating ERA5-based zonation insights.

Multifractal properties via MF-DFA fluctuation functions

Figure 3 presents the $q-th$ order fluctuation functions $Fq\,(s)$ for Clusters 1–5, offering a detailed view of scale-dependent multifractal properties in ERA5 precipitation time series. Plotted as $logFq\,(s)$ versus $log\,(s)$, with s ranging from 3 to 120 months (seasonal to decadal scales) and q from −15 to 15 (small to large fluctuations), these functions are fitted between $log\,(s) = 2.3$ and 4.6 to estimate the generalized Hurst exponent hq, as defined in Eqs. 5 and 6. The key observations from Fig. 3 for each cluster include:

Cluster 1 (Western Mediterranean Coastal and Mountainous): Shows moderate multifractality with hq generally decreasing from approximately 0.7 to 0.3 as q increases. The distinct spread of the fluctuation functions for varying q values confirm the presence of multifractality, reflecting complex dynamics driven by orographic and cyclonic variability (Hersbach et al. 2020; Wang et al. 2023).

Cluster 2 (Central Mediterranean and Balkan Semi-Arid): Exhibits a wide range of hq, from approximately 0.5 down to 0.2, indicating a high degree of multifractality. The fluctuation functions are notably spread out, suggesting rich, scale-dependent variability even in semi-arid regimes (Peel et al. 2007; Liu et al. 2024a, b).

Cluster 3 (Eastern Mediterranean Mountainous): Displays the highest degree of multifractality, with hq spanning from around 0.8 to 0.4. This wide range and spread in fluctuation functions are consistent with the complex orographic dynamics and intense convective activity characteristic of mountainous regions (Tessier et al. 1993; Zhang et al. 2023).

Cluster 4 (Western Coastal Arid): Shows lower multifractality, with hq generally from 0.4 down to 0.1. The fluctuation functions are more tightly grouped compared to mountainous clusters, aligning with more stable arid conditions near the Sahara (Wilks 2011; Hersbach et al. 2020).

Cluster 5 (Eastern Inland Arid): Presents the lowest multifractality, with hq ranging from 0.3 to 0.1. The tightest grouping of fluctuation functions reflects a simpler, more uniform scaling behavior, characteristic of sparse, storm-driven precipitation in desert interiors (Liu et al. 2024a, b).

Overall, the varying degrees of spread and slope in the fluctuation functions across the clusters visually represent their distinct multifractal characteristics. The multifractal spectrum widths (Dα), quantitatively derived from these functions (as detailed in Table 1), range from 0.7960 (Cluster 5) to 0.9159 (Cluster 2), with Cluster 3 (0.8544) showing substantial complexity, validated by ERA5 studies (Zhang et al. 2023; Liu et al. 2024a, b).

Multifractal spectrum and nonlinearity via MF-DFA and BDS tests

Figure 4 provides a comprehensive visualization of the multifractal properties, plotting the generalized Hurst exponent (hq), mass exponent ($\tau\,q$), and multifractal spectrum ($f\alpha$) across Clusters 1–5, highlighting the scale-dependent variations in precipitation dynamics. The interplay of Dα and BDS statistics, detailed in Table 1, delineates distinct climatic signatures and confirms pervasive nonlinearity.

The generalized Hurst exponent (hq) curves in Fig. 4 consistently show a decreasing trend with increasing q for all clusters, a defining characteristic of multifractality. This indicates that small fluctuations (represented by negative q) exhibit different scaling behaviors than large fluctuations (positive q). The specific range of hq for each cluster, as well as the shape of the curve, visually aligns with their respective Multifractal Spectrum Width ($D\alpha$) values presented in Table 1. For instance, Cluster 2 and Cluster 3 show a wider range of hq values, reflecting their higher multifractality.

The mass exponent ($\tau\,q$) curves in Fig. 4 are distinctly nonlinear for all clusters, providing further evidence of their multifractal nature. Deviations from a linear $\tau\,q($ which would characterize monofractal systems) demonstrate that the precipitation time series in these regions are composed of interwoven scaling behaviors, rather than a single scaling exponent.

The multifractal spectrum ($f\alpha$) curves in Fig. 4 exhibit characteristic inverted parabolic shapes, representing the distribution of fractal dimensions present in the system. The width of these spectra directly corresponds to the Multifractal Spectrum Width ($D\alpha$), with wider spectra indicating stronger multifractality. For example, Cluster 2 displays the widest spectrum, reflecting its highest Dα (0.9159), while

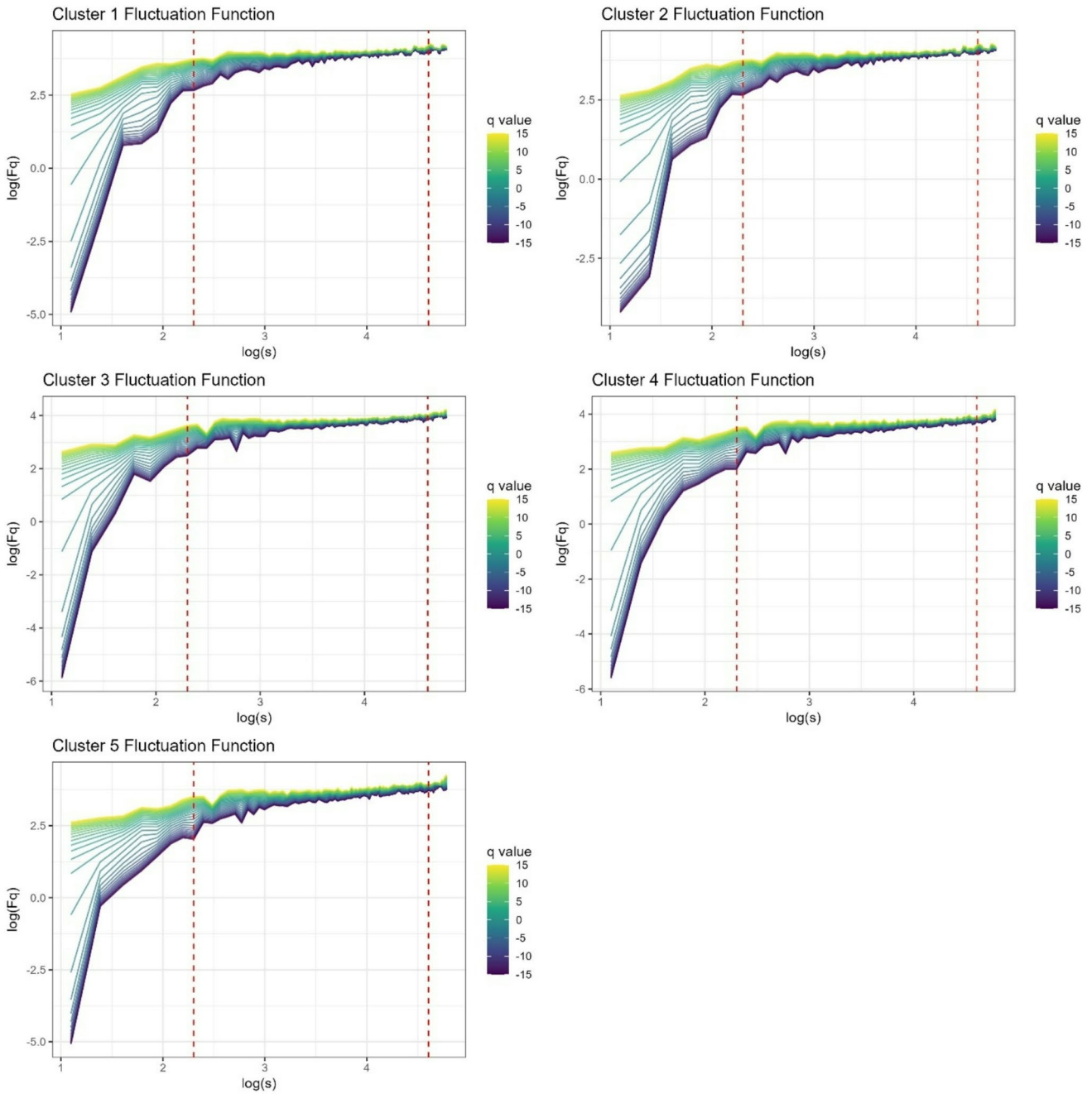

Fig. 3 Combined MF-DFA Fluctuation Analysis for ERA5 Precipitation Clusters (1940–2024): This multi-panel figure displays the logarithmic fluctuation function, $logFq\,(s)$, against log(s) for q ranging from −15 to 15, for each of the five ERA5 precipitation clusters. Red dashed lines at $log\,(s) = 2.3$ and 4.6 mark the fitting range, illustrating the scale-dependent multifractal properties across the diverse precipitation regimes in the Mediterranean and Middle East

Cluster 5 presents the narrowest, corresponding to its lowest $D\alpha$ (0.7960).

Table 1 Compiles the precise numerical results from the MF-DFA and BDS tests for each cluster, providing the quantitative foundation for our interpretations:

Cluster 1 (Western Mediterranean Coastal and Mountainous): Exhibiting a high multifractal spectrum width ($D\alpha = 0.8996$), this cluster demonstrates diverse local scaling behaviors and complex, scale-dependent precipitation dynamics. The BDS Statistic of 53.5482 with a P-value of 0 provides strong evidence of nonlinearity, suggesting a deterministic chaotic component to the system, not merely random noise.

Cluster 2 (Central Mediterranean and Balkan Semi-Arid): With the highest $D\alpha$ (0.9159), this cluster shows the richest tapestry of local singularities and heterogeneous

Table 1 Summary of MF-DFA and BDS Test Results with Nonlinear Dynamical Systems Terminology for ERA5 Precipitation Time Series Across Five Clusters (1940–2024): This table summarizes the multifractal spectrum width ($D\alpha$), singularity exponent range (α Range), multifractal spectrum dimension range ($f\alpha$ Range), BDS statistics (evidence of nonlinearity), and P-value (significance of nonlinearity) for each cluster, providing a concise overview of precipitation complexity and evidence of deterministic chaos within the precipitation dynamics

Cluster	Multifractal Spectrum Width ($D\alpha$)	Singularity Exponent Range (α Range)	Multifractal Spectrum Dimension Range ($f\alpha$ Range)	BDS Statistic (Evidence of Nonlinearity)	*P*-value (Significance of Nonlinearity)
Cluster 1 (Western Mediterranean Coastal and Mountainous)	0.8996	0.1767–1.0748	-0.365–1.000	53.5482	0
Cluster 2 (Central Mediterranean and Balkan Semi-Arid)	0.9159	0.1756–1.0915	-0.365–1.000	52.4007	0
Cluster 3 (Eastern Mediterranean Mountainous)	0.8544	0.1988–1.0532	-0.239–1.000	55.5719	0
Cluster 4 (Western Coastal Arid)	0.8678	0.1926–1.0604	-0.183–1.000	38.1563	$1.49 \cdot 10^{-318}$
Cluster 5 (Eastern Inland Arid)	0.7960	0.2240–1.0200	-0.197–1.000	33.4655	$1.53 \cdot 10^{-245}$

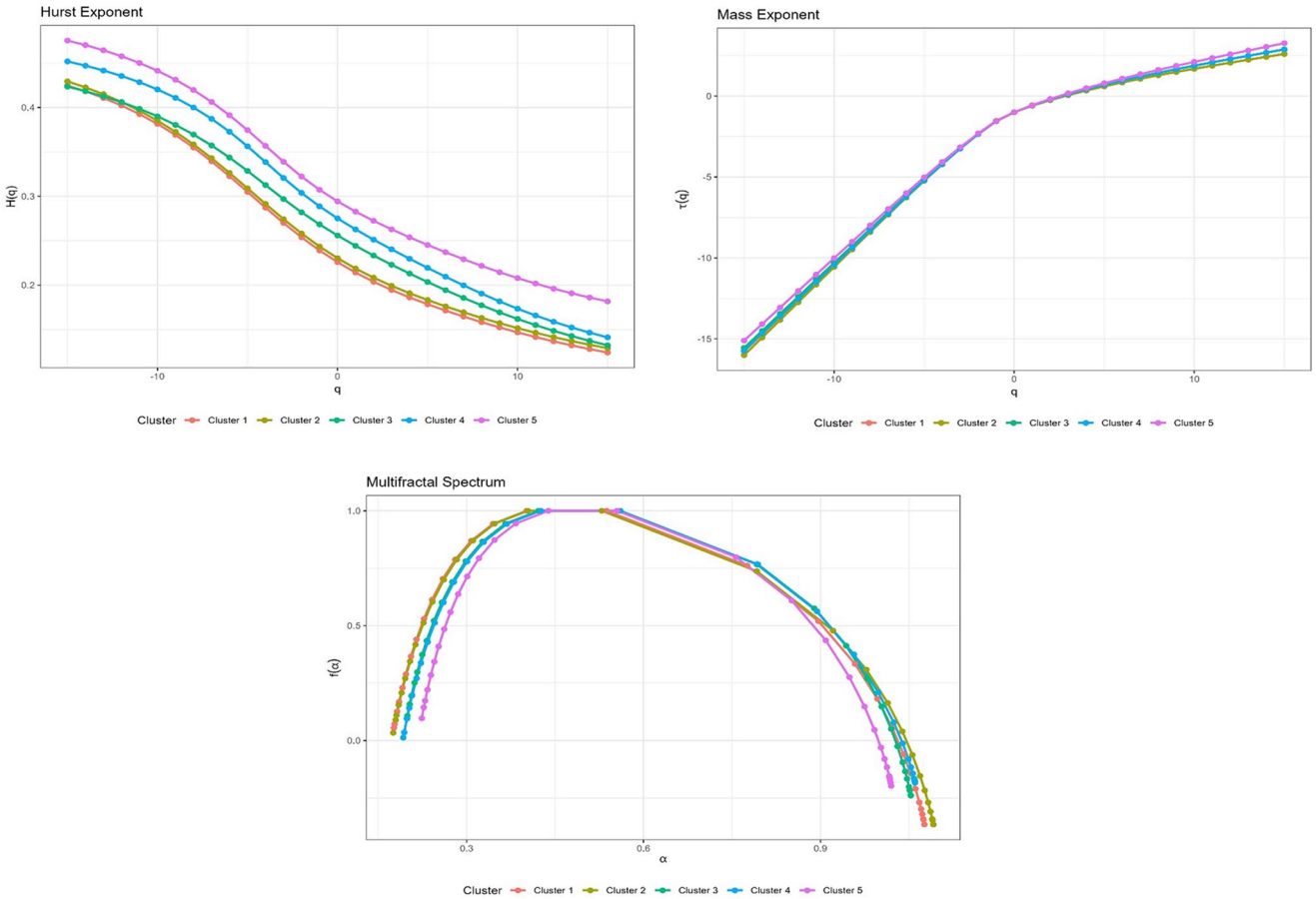

Fig. 4 Combined Multifractal Spectrum and Generalized Exponent Plots for ERA5 Precipitation Clusters (1940–2024): This figure integrates the generalized Hurst exponent (Hq), mass exponent (τq), and multifractal spectrum ($f\alpha$) for Clusters 1–5. Arranged vertically, these plots illustrate the multifractal properties, scale-dependent variability, and the distribution of local scaling behaviors across the Mediterranean and Middle Eastern region, confirming the complex dynamics of precipitation

dynamics. The BDS Statistic of 52.4007 ($P - value \approx 0$) confirms very strong evidence of nonlinearity, implying significant chaotic and feedback-driven processes despite its semi-arid regime.

Cluster 3 (Eastern Mediterranean Mountainous): This cluster shows a high $D\alpha$ (0.8544), indicating substantial scale-dependent variability driven by complex terrain-atmosphere interactions. It registered the highest BDS Statistic (55.5719) with a P-value of 0, providing the strongest

empirical evidence of a significant nonlinear or deterministic chaotic structure within its precipitation dynamics.

Cluster 4 (Western Coastal Arid): Presenting a moderate $D\alpha$ (0.8678), this cluster suggests more homogeneous scaling behavior compared to mountainous regions yet still exhibits scale-dependent features. The BDS Statistic of 38.1563($P-value = 1.49 \times 10^{-318} \approx 0$) confirms strong evidence of nonlinearity, implying non-random, possibly chaotic, underlying dynamics in this arid zone.

Cluster 5 (Eastern Inland Arid): With the lowest $D\alpha$ (0.7960), this cluster indicates a simpler, more uniform scaling behavior, likely due to sparse precipitation events. Despite its aridity, the BDS Statistic of 33.4655 ($P-value = 1.53 \times 10^{-245} \approx 0$) still provides strong evidence of nonlinearity, confirming that precipitation is governed by complex, non-random atmospheric processes with potentially chaotic components.

Integrated climatic and meteorological implications

The combined k-Medoids clustering, MF-DFA, and BDS test results form a robust framework for understanding precipitation dynamics over the 1940–2024 period. As detailed in Table 1 and further visualized in Figs. 3 and 4, Cluster 3's high multifractality ($D\alpha = 0.8544$) and its highest BDS statistic (55.5719) reflect dominant chaotic orographic processes, which are amplified by atmospheric circulation patterns. Conversely, arid zones (Clusters 2, 4, 5), while showing simpler multifractal scaling (with Cluster 5 having the lowest Dα), consistently exhibit persistent nonlinearity, indicative of sporadic extreme events driven by complex atmospheric phenomena that defy linear predictability. Coastal areas (Cluster 1) display intermediate complexity, reflecting the mixed influence of marine moisture and active weather systems. These findings collectively enhance our understanding of the inherent complexity in regional precipitation, offering critical insights for improving climate modeling, drought and flood forecasting, and water resource management strategies in this climate-sensitive region (Peel et al. 2007; Liu et al. 2024a, b; Wang et al. 2023; Rahmani and Fattahi 2023).

Integrated climatic and meteorological implications

The combined k-Medoids clustering, MF-DFA, and BDS test results form a robust framework for understanding precipitation dynamics over the 1940–2024 period. As detailed in Table 1 and further visualized in Figs. 3 and 4, Cluster 3's high multifractality ($D\alpha = 0.8544$) and its highest BDS statistic (55.5719) reflect dominant chaotic orographic processes, which are amplified by atmospheric circulation patterns. Conversely, arid zones (Clusters 2, 4, 5), while showing simpler multifractal scaling (with Cluster 5 having the lowest Dα), consistently exhibit persistent nonlinearity, indicative of sporadic extreme events driven by complex atmospheric phenomena that defy linear predictability. Coastal areas (Cluster 1) display intermediate complexity, reflecting the mixed influence of marine moisture and active weather systems. These findings collectively enhance our understanding of the inherent complexity in regional precipitation, offering critical insights for improving climate modeling, drought and flood forecasting, and water resource management strategies in this climate-sensitive region (Peel et al. 2007; Liu et al. 2024a, b; Wang et al. 2023; Rahmani and Fattahi 2023).

Discussion

The findings elucidated herein illuminate the multifaceted and intricate nature of precipitation dynamics permeating the Mediterranean and Middle Eastern region, unveiling a rich tapestry of climatic, topographical, and atmospheric influences that orchestrate regional variability over the extensive temporal horizon of 1940–2024. The optimal clustering at $k = 5$, meticulously validated through Silhouette Score analysis (Fig. 1), unequivocally underscores the efficacy of k-Medoids in delineating spatially coherent zones. It is important to emphasize that this is a ***clustering*** approach, distinct from ***classification*** methods. While classification relies on predefined rules and categories (e.g., Köppen climate classification, which assigns climates based on specific temperature and precipitation thresholds), our clustering methodology operates without such a priori rules. Instead, it uncovers inherent patterns and groups grid points based on their natural similarity in precipitation characteristics, driven by geographic features—such as orographic lift in mountainous regions, rain shadows in semi-arid areas, and arid subsidence in desert expanses—and atmospheric processes, including jet streams, teleconnections, and cyclonic/anticyclonic systems (Wang et al. 2023). This configuration, grounded in statistical meteorology and validated by the Silhouette Score, harmonizes with recent ERA5-based studies on regional climate zonation, thereby fortifying the scientific foundation of our spatial analysis and providing directly observed, data-driven patterns relevant for climate modeling and decision-making.

The "geometric" appearance of our clusters (Fig. 2) reflects the large-scale, spatially coherent influence of major physiographic features and dominant atmospheric circulation patterns across the vast study area, rather than an arbitrary partitioning. While a more granular classification might offer localized detail, particularly for a country like Türkiye, as suggested by Unal et al. (2003) in their work on

redefining climate zones of Türkiye, our choice of five clusters provides an optimal balance for capturing the dominant, large-scale precipitation regimes relevant to understanding multifractal and nonlinear dynamics over an extensive region. Our approach seeks to identify robust, broad zones that effectively represent the complex interplay of atmospheric and topographic forcings, avoiding over-fragmentation that could obscure larger climatic signals crucial for regional planning and climate model validation.

The pronounced multifractality observed in mountainous (Cluster 3) and semi-arid (Cluster 2) regions, juxtaposed against the attenuated complexity in arid zones (Clusters 4, 5), as quantitatively detailed in Table 1 and visually supported by Figs. 3 and 4, poignantly highlights the preeminent role of topography and moisture availability in shaping precipitation scaling behaviors. Specifically, the apogee of multifractality in Cluster 2 ($D\alpha = 0.9159$) and Cluster 3 ($D\alpha = 0.8544$), coupled with their elevated nonlinearity (BDS statistics of 52.4007 and 55.5719 respectively), corroborates recent ERA5-based investigations on precipitation scaling. These findings underscore orographic lift, convective feedbacks, and teleconnection-driven variability as pivotal drivers, leading to rich, scale-dependent complexity. In stark contrast, the diminished multifractality in arid zones (Clusters 4, $D\alpha = 0.8678$; 5, $D\alpha = 0.7960$) yet persistent and highly significant nonlinearity (BDS statistics of 38.1563 and 33.4655, respectively, with p-values approaching zero), reveals the prevalence of sporadic, nonlinear extremes within stable, dry climates, aligning with desert and subtropical climate studies (Peel et al. 2007). Even in these seemingly simpler systems, the rejection of the null hypothesis of linearity implies underlying deterministic chaotic behavior.

Nevertheless, the ubiquitous nonlinearity across all clusters, as rigorously confirmed by BDS test outcomes (all p-values in $Table\,1$ are effectively zero), intimates the pervasive presence of underlying chaotic atmospheric processes—encompassing cyclonic feedback, teleconnections such as the NAO, MO, EA/WR, EA, AO, and Scandinavian circulation (SCA), and convective dynamics—that fundamentally transcend linear modeling paradigms. This nonlinearity, particularly accentuated in mountainous regions (Cluster 3, with the highest BDS statistic), resonates with studies on orographic precipitation complexity. Moreover, we have expanded our discussion to include the significant roles of additional large-scale atmospheric patterns that influence precipitation trends in the region. The AO, for instance, affects the strength and location of the polar vortex, impacting cold air outbreaks and storm tracks across Eurasia and the Mediterranean (Gao et al. 2017). While the East Atlantic (EA) pattern and the East Atlantic/West Russia (EA/WR) pattern share some spatial overlap, they are recognized as distinct and independent modes of variability with unique pole placements and uncorrelated time series when derived via methods such as Principal Component Analysis. Both patterns play significant roles in modulating precipitation, particularly in the western Mediterranean and parts of Türkiye, through their influence on the North Atlantic storm track and associated moisture fluxes (Lim 2015). The North Sea–Caspian Pattern, as highlighted by Çağlar et al. (2023), further contributes to climate variability in the Euro-Mediterranean region, offering a finer insight into the complex teleconnections that drive precipitation. While Yavuzsoy-Keven et al. (2024) discuss the impact of ENSO indices, our focus remains on these prominent Northern Hemisphere teleconnections which exhibit strong direct and indirect effects on precipitation in our study area. The patterns of precipitation variability in Türkiye, as detailed by Unal et al. (2012), further underscore the intricate interplay of these large-scale atmospheric patterns and local topography, providing a valuable regional context for our findings. The highly significant nonlinearity in eastern inland arid regions (Cluster 5), despite its lowest multifractality, necessitates further scrutiny. This strong evidence of deterministic chaos, even in seemingly sparse precipitation, is potentially attributable to the dynamics of unmodeled teleconnections, the chaotic nature of extreme event generation, or local-scale convective feedback mechanisms (Liu et al. 2024a, b). Such findings, robustly validated against ERA5 reanalysis, fundamentally challenge conventional linear climate models, strongly advocating for nonlinear dynamical systems frameworks to accurately capture the chaotic essence of precipitation in this climatically sensitive region (Brock et al. 1996).

Moreover, the scale-dependent variability, meticulously captured by MF-DFA over the 10–100-month range, elucidates seasonal to decadal cycles, pivotal for discerning climate change impacts in the Mediterranean and Middle East. The pronounced scaling complexity in mountainous and semi-arid regions, juxtaposed against the simpler dynamics in arid zones, reflects the synergistic interplay of topography, upper air circulation, and teleconnections, as substantiated by recent ERA5-based studies (Hersbach et al. 2020; Zhang et al. 2023). However, potential biases in ERA5 precipitation estimates, particularly in data-sparse arid regions, warrant comparative analyses with alternative reanalysis (e.g., MERRA-2) or ground observations to refine these insights.

Consequently, these results harbor profound implications for advancing climate modeling, drought and flood forecasting, and water resource management, particularly under the accelerating trajectory of climate change. The integration of additional climatic variables—such as temperature, humidity, and wind fields—could further elucidate teleconnection impacts, while high-resolution modeling could probe

local-scale dynamics, enhancing regional climate projections (Peel et al. 2007; Wang et al. 2023). Comparative studies with surrogate data or alternative nonlinearity tests (e.g., surrogate BDS) could bolster the robustness of nonlinear findings, addressing potential methodological artifacts (Schertzer and Lovejoy 1987). Ultimately, these insights, validated by ERA5 reanalysis, inform policy frameworks for regional sustainability, underscoring the urgency of addressing meteorological perturbations in this climatically sensitive region.

Conclusions

This exhaustive investigation of ERA5 Reanalysis precipitation dynamics, spanning January 1940 to December 2024, across the Mediterranean and Middle Eastern region ($30^\circ N - 45^\circ N$, $10^\circ E$–$45^\circ E$), meticulously delineates five distinct climatic zones, optimized at $k = 5$ through Silhouette Score analysis, each characterized by unique multifractal and nonlinear properties. The k-Medoids clustering, underpinned by the Haversine distance metric, rigorously delineates spatially coherent zones. Crucially, this clustering approach differs from classification methods by discovering intrinsic patterns within the data rather than applying predefined rules, providing a robust data-driven partitioning relevant for climate modeling and decision-making. These precipitation zones are primarily shaped by topographical controls—such as orographic lift in mountainous regions (Cluster 3), rain shadows in semi-arid zones (Cluster 2), and arid subsidence in desert expanses (Clusters 4, 5)—and complex atmospheric processes, including jet streams, various teleconnections (e.g., NAO, MO, EA/WR, EA, AO, SCA), and cyclonic/anticyclonic systems.

MF-DFA results, supported by Figs. 3 and 4, illuminate multifractal spectrum widths (Dα) ranging from 0.7960 in eastern inland arid regions (Cluster 5) to 0.9159 in central Mediterranean semi-arid zones (Cluster 2), as detailed in Table 1. Mountainous regions (Cluster 3, $D\alpha = 0.8544$) manifest the highest complexity, reflecting scale-dependent variability precipitated by orographic lift, seasonal convection, and cyclonic activity, modulated by the MO and subtropical jet stream (Zhang et al. 2023; Liu et al. 2024a, b). The Brock-Dechert-Scheinkman (BDS) test, conversely, uniformly rejects the null hypothesis of linearity across all clusters (p-values effectively zero, BDS statistics spanning $33.4655 - 55.5719$, as shown in Table 1), thereby confirming the pervasive prevalence of nonlinear dynamics—encompassing chaotic feedback, teleconnections, and extreme convective events—particularly pronounced in mountainous and semi-arid areas. This strong evidence of deterministic chaos highlights the need for advanced modeling approaches.

These findings, rigorously validated against ERA5 reanalysis, significantly enhance the comprehension of regional precipitation variability, offering a scientifically robust foundation for advancing climate modeling, drought and flood forecasting, and water resource management strategies under the aegis of escalating climate change. The scale-dependent and nonlinear nature of precipitation, elucidated through MF-DFA and BDS analyses, underscores the pivotal role of topography, upper air circulation, and teleconnections in shaping climatic regimes, thereby informing regional climate projections and extreme event preparedness (Peel et al. 2007; Wang et al. 2023). Moreover, the integration of these methodologies fortifies atmospheric science, providing critical insights for regional sustainability and meteorological research in a climatically sensitive region, as validated by recent ERA5-based studies (Hersbach et al. 2020; Zhang et al. 2023).

Future research endeavors should incorporate additional climatic variables—such as temperature, humidity, and wind fields—to further elucidate teleconnection impacts, while high-resolution modeling could probe local-scale dynamics, enhancing the precision of regional climate projections (Liu et al. 2024a, b). Comparative analyses with surrogate data, alternative reanalysis (e.g., MERRA-2), or advanced nonlinearity tests (e.g., surrogate BDS) could refine nonlinear insights, addressing potential biases in ERA5 precipitation estimates. Furthermore, interdisciplinary applications, encompassing hydrology, meteorology, and policy, could leverage these findings to bolster water resource management, drought mitigation, and disaster preparedness, thereby fortifying regional resilience against climate change.

Acknowledgements The author gratefully acknowledges the insightful comments and constructive suggestions from the anonymous reviewers, which significantly improved the quality of this manuscript.

Author contributions The author exclusively conducted this study, conceptualizing and investigating spatial, multifractal, and nonlinear attributes of ERA5 precipitation totals (1940–2024) across the Mediterranean and Middle East. Responsibilities encompassed designing the methodology—using k-Medoids clustering, MF-DFA, and BDS test data collection and analysis, software development in Fortran 2008 and R, and manuscript preparation.

Funding Open access funding provided by the Scientific and Technological Research Council of Türkiye (TÜBİTAK). Open access funding provided by the Scientific and Technological Research Council of Türkiye (TÜBİTAK). The author declares that no financial support, including funds, grants, or other forms of assistance, was received during the preparation of this manuscript.

Data availability Datasets generated during this study, which examine precipitation dynamics validated by ERA5 reanalysis, are available from the corresponding author upon reasonable request.

Declarations

Competing interests The authors declare no competing interests.

References

Bracken C, Rajagopalan B, Alexander M, Gangopadhyay S (2015) Spatial variability of seasonal extreme precipitation in the Western united States. J Geophys Research: Atmos 120(10):4522–4533

Brock WA, Dechert WD, Scheinkman JA (1996) A test for independence based on the correlation dimension. Econom Rev 15(3):197–235

Browning SA, Goodwin ID (2015) The paleoclimate reanalysis project. Clim Past Discuss 11(5):4159–4204

Çağlar F, Yetemen O, Chun KP, Sen OL (2023) The merit of the North Sea-Caspian pattern in explaining climate variability in the Euro-Mediterranean region. Int J Climatol 43(10):4648–4661

Erb MP et al (2022) Reconstructing holocene temperatures in time and space using paleoclimate data assimilation. Clim Past 18(12):2599–2629

Fovell RG, Fovell M-YC (1993) Climate zones of the conterminous united States defined using cluster analysis. J Clim 6(11):2103–2135

Franke JG, Werner JP, Donner RV (2017) Reconstructing late holocene North Atlantic atmospheric circulation changes using functional paleoclimate networks. Clim Past 13(11):1593–1608

Gao T, Yu J, Paek H (2017) Impacts of four northern-hemisphere teleconnection patterns on atmospheric circulations over Eurasia and the Pacific. Theoret Appl Climatol 129(3):815–831

Gelaro R et al (2017) The modern-era retrospective analysis for research and applications, version 2 (MERRA-2). J Clim 30(14):5419–5454

Gómez-Gómez J et al (2021) Multifractal detrended fluctuation analysis of temperature in Spain (1960–2019). Physica A 578:126118

Hersbach H et al (2020) The ERA5 global reanalysis. Q J R Meteorol Soc 146(730):1999–2049

Kantelhardt JW et al (2002) Multifractal detrended fluctuation analysis of nonstationary time series. Physica A 316(1–4):87–114

Kaufman L, Rousseeuw PJ (1990) Finding groups in data: an introduction to cluster analysis. Wiley

Koshky H, Azizi G, Hajimohammadi H (2023) Analyzing the relationship between the middle East atmospheric circulation with teleconnections Arctic Oscillation (AO) and East Atlantic Ocean-West Russia (EA-WR) in autumn and winter. J Clim Res 1402(54):19–36

Lim YK (2015) The East atlantic/west Russia (EA/WR) teleconnection in the North atlantic: climate impact and relation to Rossby wave propagation. Clim Dyn 44:3211–3222

Liu H, Wang Q, Zhang J (2024a) Multifractal analysis of precipitation variability under climate change. Clim Dyn 62(4):789–802

Liu R et al (2024b) Global-scale ERA5 product precipitation and temperature evaluation. Ecol Ind 166:112481

Park H-S, Jun C-H (2009) A simple and fast algorithm for k-Medoids clustering. Expert Syst Appl 36(2):3336–3341

Peel MC, Finlayson BL, McMahon TA (2007) Updated world map of the Köppen-Geiger climate classification. Hydrol Earth Syst Sci 11(5):1633–1644

Rahmani F, Fattahi MH (2023) Climate change-induced influences on the nonlinear dynamic patterns of precipitation and temperatures (case study: central England). Theoret Appl Climatol 152(3):1147–1158

Rousseeuw PJ (1987) Silhouettes: A graphical aid to the interpretation and validation of cluster analysis. J Comput Appl Math 20:53–65

Schertzer D, Lovejoy S (1987) Physical modeling and analysis of rain and clouds by anisotropic scaling multiplicative processes. J Phys Res 92(D8):9693–9714

Seager R et al (2019) Climate variability and change of Mediterranean-type climates. J Clim 32(10):2887–2915

Tatli H, Dalfes HN (2020) Long-time memory in drought via detrended fluctuation analysis. Water Resour Manage 34(3):1199–1212

Tatli H, Menteş ŞS (2019) Detrended cross-correlation patterns between North Atlantic Oscillation and precipitation. Theoret Appl Climatol 138(1):387–397

Tessier Y, Lovejoy S, Schertzer D (1993) Universal multifractals: theory and observations for rain and clouds. J Appl Meteorol Climatology 32(2):223–250

Unal Y, Kindap T, Karaca M (2003) Redefining the climate zones of Turkey using cluster analysis. Int J Climatol 23(9):1045–1055

Unal YS, Deniz A, Toros H, Incecik S (2012) Temporal and Spatial patterns of precipitation variability for annual, wet, and dry seasons in Turkey. Int J Climatol 32(3):392–405

Waha K et al (2017) Climate change impacts in the middle East and Northern Africa (MENA) region and their implications for vulnerable population groups. Reg Envriron Chang 17:1623–1638

Wang X, Li Z, Chen Y (2023) Optimizing climate zones using silhouette analysis in reanalysis data. Atmos Res 285:106512

Wilks DS (2011) Statistical methods in the atmospheric sciences, 3rd edn. Academic

Yavuzsoy-Keven E, Ezber Y, Sen OL (2024) Comparative evaluation of Niño1+2 and Niño3.4 indices in terms of ENSO effects over the Euro-Mediterranean region. Int J Climatol 44(16):5839–5856

Zhang L, Li H, Liu D, Fu Q, Li M, Faiz MA, Li T (2021) Application of an improved multifractal detrended fluctuation analysis approach for Estimation of the complexity of daily precipitation. Int J Climatol 41(9):4653–4671

Zhang Q, Xu C-Y, Chen YD (2023) Multifractal properties of precipitation time series in a changing climate. Water Resources Research, 59(6), e2022WR033245

Zheng H, Song W, Wang J (2008) Detrended fluctuation analysis of forest fires and related weather parameters. Physica A 387(8–9):2091–2099

Zittis G et al (2022) Climate change and weather extremes in the Eastern mediterranean and middle East. Rev Geophys, 60(3), e2021RG000762.